american physiological society

JNP JOURNAL OF NEUROPHYSIOLOGY

J Neurophysiol 133: 1423–1434, 2025.
First published April 7, 2025; doi:10.1152/jn.00459.2024

RESEARCH ARTICLE

Control of Movement

Single and paired TMS pulses engage spatially distinct corticomotor representations in human pericentral cortex

Mads A. J. Madsen,[1] Lasse Christiansen,[1,2] Chloe Chung,[1,3] Morten G. Jønsson,[1] and Hartwig R. Siebner[1,4,5]

[1]*Danish Research Centre for Magnetic Resonance, Copenhagen University Hospital Amager & Hvidovre, Hvidovre, Denmark;* [2]*Department of Neuroscience, Faculty of Health and Medical Sciences, University of Copenhagen, Copenhagen, Denmark;* [3]*Physiotherapy Department, Tan Tock Seng Hospital, Singapore;* [4]*Department of Neurology, Copenhagen University Hospital Bispebjerg & Frederiksberg, Copenhagen, Denmark; and* [5]*Institute for Clinical Medicine, Faculty of Health and Medical Sciences, University of Copenhagen, Copenhagen, Denmark*

Abstract

Single-pulse transcranial magnetic stimulation (TMS) of the primary motor hand area can assess corticomotor function in humans by evoking motor-evoked potentials (MEPs). Paired-pulse TMS at peri-threshold intensity elicits short-latency intracortical facilitation (SICF) with early peaks at interpulse intervals of 1.0–1.8 ms ($SICF_1$) and 2.4–3 ms ($SICF_2$). The similarity between the periodicity of SICF and indirect (I-)waves in the corticospinal volleys evoked by single-pulse TMS suggests that SICF originates from I-wave generating circuits. This study aimed to explore the mechanisms of MEP generation by mapping the corticomotor representations of single-pulse and paired-pulse TMS targeting $SICF_1$ and $SICF_2$ peaks. We performed central sulcus shape-based, robot-assisted and neuro-navigated motor maps in 14 participants (7 females). MEPs were recorded from two hand muscles and the spatial properties of each corticomotor map were analyzed. For both hand muscles, we found a consistent posterior shift of the center of gravity (CoG) for SICF maps compared with single-pulse maps, with a larger shift for $SICF_1$. CoG displacement in the $SICF_1$ map correlated with individual $SICF_1$ latencies. Furthermore, abductor digiti minimi (ADM) maps consistently peaked more medially than first dorsal interosseus (FDI) maps and paired-pulse TMS resulted in larger corticomotor maps than single-pulse TMS. This is the first study to show that circuits responsible for SICF have a more posterior representation in the precentral crown than those generating MEPs via single-pulse TMS. These findings indicate that paired-pulse TMS probing $SICF_1$, $SICF_2$, and single-pulse TMS engage overlapping but spatially distinct cortical circuits, adding further insights into the intricate organization of the human motor hand area.

NEW & NOTEWORTHY Single- and paired-pulse transcranial magnetic stimulation (TMS) is widely used to study corticomotor physiology in humans, but do they engage the same intracortical circuits? We compared the spatial properties of corticomotor maps elicited by single-pulse TMS to those elicited by paired-pulse short-latency intracortical facilitation (SICF). SICF maps consistently showed a posterior shift in center of gravity compared with single-pulse maps, suggesting that paired-pulse TMS engages cortical circuits that are spatially distinct from single-pulse TMS.

I-waves; motor mapping; short-interval intracortical facilitation; somatotopy; transcranial magnetic stimulation

INTRODUCTION

Transcranial magnetic stimulation (TMS) of the hand motor representation in the precentral gyrus can cause a contraction of contralateral hand muscles, making TMS a powerful noninvasive tool to probe corticomotor physiology. Exactly which cortical elements are stimulated by TMS is still unknown, but biophysical modeling of morphologically realistic cortical neurons suggests that myelinated axon terminals from pyramidal cells and inhibitory interneurons in the crown of the gyri constitute low-threshold targets for TMS (1–3). Interestingly, anatomical tracer studies in nonhuman primates show that the

Correspondence: M. A. J. Madsen (madsjm@drcmr.dk); H. R. Siebner (h.siebner@drcmr.dk).
Submitted 8 October 2024 / Revised 21 November 2024 / Accepted 1 April 2025

primary output region of monosynaptic pyramidal tract neurons (PTNs) in the primary motor cortex lies in the evolutionary younger, posterior part of Broadmann's area 4, which is typically located in the sulcal wall or fold (4). In addition, human epidural recordings show that TMS elicits both a direct descending wave followed by a number of later indirect (I)-waves (5) suggesting that populations of PTNs are activated trans-synaptically and experience numerous discharges from a single TMS pulse. The notion is supported by paired-pulse TMS protocols where an additional TMS pulse (usually subthreshold) is used to condition the response to the single TMS pulse alone, often resulting in marked changes in peak-to-peak amplitude of the motor-evoked potential (MEP) (6, 7). For example, two TMS pulses delivered in very close temporal proximity i.e., interstimulus intervals (ISIs) of ~1–5 ms markedly facilitate the MEP as compared with single-pulse TMS (8). This phenomenon, coined short-latency intracortical facilitation (SICF) (9), is cortically mediated (9, 10) and more pronounced when ISIs mimic the periodicity of the I-waves observable in epidural recordings, although also detectable at SICF trough ISIs with higher stimulation intensity or more pulses (11).

Because the periodicity of SICF matches that of epidurally recorded I-waves, the general hypothesis is that SICF works through facilitation of the I-wave generating circuits that are also involved in generating single-pulse MEPs. However, the exact cortical networks involved in generating single-pulse MEPs and SICF and their similarities are still unknown. Moreover, several findings suggest that the first and second SICF peaks ($SICF_1$ and $SICF_2$) may reflect activity in nonidentical cortical circuits that subserve distinct sensorimotor functions (12–14). Although substantial effort has been made to pinpoint the most likely site of cortical activation by single-pulse TMS (3), the spatial location of the intraneuronal networks underpinning SICF remains entirely unexplored.

The objective of this study was to map the spatial cortical representation of single-pulse TMS and SICF to test whether spatially distinct or identical cortical populations underpin these phenomena. Our hypothesis was that paired-pulse SICF engages different neural populations, compared with single pulse, evident as a systematic difference in the center of gravity (CoG) of the corticomotor maps. In addition, we hypothesized that there would be a spatiotemporal relationship between the spatial displacement and the ISIs of the first and the second SICF peak. To test these hypotheses, we mapped the peri-central corticomotor representations of intrinsic hand muscles with single-pulse TMS and two SICF conditions with ISIs adjusted to the individual $SICF_1$ and $SICF_2$ peak latency, respectively. We used central sulcus shape-based mapping (15, 16) as it provides higher sensitivity toward muscular somatotopy compared with standard grid-based mapping (16, 17) and is sensitive toward between-subject variability in hotspot location (18).

MATERIALS AND METHODS

Experimental Design

Before the experimental TMS session, participants underwent a structural T1-weighted magnetic resonance imaging (MRI) scan, which was used to plan TMS targets for sulcus-shaped mapping (16). In the experimental session, participants went through recordings of SICF curves to determine individual latencies of SICF peaks. Following this, three different robot-assisted, neuro-navigated, sulcus-shaped TMS motor maps were created using single- or paired-pulse TMS targeting either the first or the second SICF peak (Fig. 1).

Participants

Seventeen healthy right-handed volunteers (mean age: 26.9 yr, 8 females) participated in the study. Handedness was assessed by the Edinburgh handedness inventory (19). All participants had no history of psychiatric disorders and were screened for contraindications to TMS (20). Written informed consent was obtained from all subjects and studies were performed in accordance with the Helsinki declaration on Human experimentation. The study was approved by the Ethics Committees of the Capital Region of Denmark (H-15000551). Two participants were excluded from the study due to continuous background contractions on the

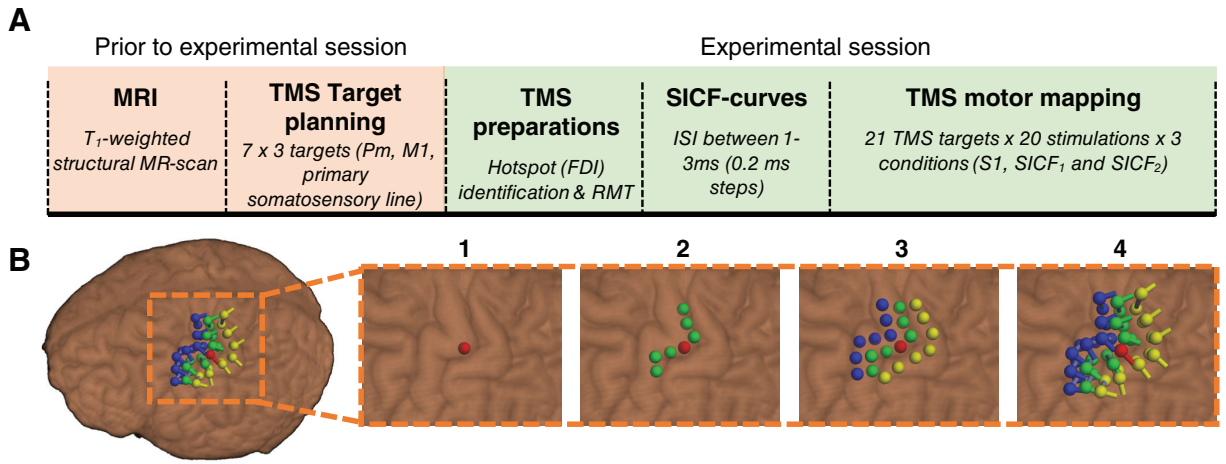

Figure 1. Experimental design and protocol. *A*: flow chart of the experimental procedure. *B*: map planning in the neuronavigation software for the robot-assisted transcranial magnetic stimulation (TMS) motor mapping. FDI, first dorsal interosseous; M1, primary motor cortex; MRI, magnetic resonance imaging; Pm, premotor cortex; S1, single-pulse; SICF, short-latency intracortical facilitation.

electromyography (EMG) recordings and one participant was excluded due to a too high resting motor threshold (RMT) [>91% maximal stimulator output (MSO)]. Thus, 14 subjects (7 females) were included in the statistical analyses.

Magnetic Resonance Imaging

Prior to the experimental session, a three-dimensional (3-D) T1-weighted magnetization-prepared rapid gradient-echo (MPRAGE) MRI scan was acquired on a 3-T Verio scanner (Siemens, Erlangen, Germany) with the following parameters: repetition time (TR)/echo time (TE) = 2,300/2.98 ms, T1 = 1,100 ms; 256 × 256 matrix, flip angle 9°, 1 mm^3 isotropic voxel.

Surface Electromyography

Electrical muscle activity of the right first dorsal interosseus (FDI) and abductor digiti minimi (ADM) muscles were recorded with surface electrodes (Ambu Neuroline 700, Ballerup, Denmark) using a bipolar belly-tendon montage. The Analog EMG signal was filtered (band-pass, 5–2,000 Hz), amplified (1,000×, D360, Digitimer, Letchworth Garden City, UK), digitalized (sampling frequency 5,000 Hz, 1201 micro Mk-II, Cambridge Electronic Design, Cambridge, UK), recorded (Signal 4.0, Cambridge Electronic Design, Cambridge, UK), and stored on a computer for later off-line analysis. During the experiment, background EMG was monitored by the experimenter, and participants were instructed to relax whenever background EMG was detected.

Transcranial Magnetic Stimulation

Single- and paired-pulse TMS was delivered using a MagPro X100 with MagOption stimulator (Magventure, Skovlunde, Denmark) connected to a cooled-MC-B35 figure-of-eight coil with windings of 35 mm diameter (Magventure). For handheld TMS procedures, the coil was held ∼45° to the mid-sagittal plane with the handle facing lateral and posterior. A biphasic pulse configuration that induced an anterior-posterior followed by posterior-anterior (AP-PA) current in the cortex was selected to evoke MEPs at the lowest possible stimulation intensity (21). Pulse-width was 300 μs and held constant for all pulses. All TMS was performed using stereotactic neuronaviation (Localite, Sankt Augustin, Germany) in which individual structural MRI images were uploaded. The optimal coil position (hotspot) to activate the right FDI was identified through a mini-mapping procedure and defined as the site where TMS elicited the largest and most consistent MEPs. RMT was determined to the nearest 1% of MSO using single-pulse TMS and defined as the minimal stimulus intensity required to evoke a response of 50 μV in at least 5 of 10 successive trials (22). Following the determination of the hotspot and RMT, TMS was performed by a neuronavigation TMS robot (Axilum Robotics, Schiltigheim, France) for the remainder of the experiment.

Short-interval intracortical facilitation curves.

For paired-pulse TMS to induce SICF, the intensity of the first TMS stimulus (S1) was set to 110% RMT (determined for FDI) and to 90% RMT for the second TMS stimulus (S2) (8). An SICF curve was created before the mapping procedure to determine individual $SICF_1$- and $SICF_2$-peak latencies. ISIs ranging from 1.0 ms to 3 ms were tested in 0.2-ms steps. Ten paired TMS pulses were delivered in pseudo-random order over the FDI hotspot for each ISI together with S1 alone. The average peak-to-peak MEP amplitude was calculated online for each condition and plotted against the respective ISI. The intervals that produced the largest average peak-to-peak MEP amplitude for the FDI muscle, within the first (1–1.8 ms) and second (2.4–3 ms) SICF range were determined as individual $SICF_1$- and $SICF_2$-peak latencies.

Robot-assisted, neuro-navigated, sulcus-shaped TMS motor mapping.

TMS mapping targets. TMS mapping was done in a 3 × 7 grid centered around the hand knob of the precentral gurus (23) that was identified by a trained investigator. Seven targets were placed along the posterior part of the crown of the precentral gyrus (i.e., the gyral "lip") (see Fig. 1*B*). Each target was placed conforming with individual shape of the central sulcus to form a line (M1-line). The posterior convexity of the "hand-knob" was used as a central reference point that corresponded to target 4. Coil orientation was adjusted to produce a current direction perpendicular to the central sulcus, which has been shown to be superior for M1-mapping (16). Two additional lines were created to examine the potential antero-posterior shift of somatotopy with SICF mapping. A premotor line was positioned in accordance with the M1 line but with an anterior shift such that the targets were placed on the precentral gyral crown. In addition, seven posterior targets were placed in accordance with the M1-line but on the crown of the postcentral gyrus.

TMS motor mapping procedure. Three motor maps were conducted in the same experimental session. For each map, 20 single (S1) or paired ($SICF_1$ and $SICF_2$ condition) TMS pulses were applied to each of the 21 targets in a random order, resulting in 420 stimulations per map and a total of 1,260 stimulations. The order of the three conditions was randomized and counter-balanced across subjects and TMS pulses were delivered at a frequency of 0.25 Hz (25% jitter). SICF and single-pulse TMS maps were generated separately rather than intermixed to avoid the increased MEP amplitudes from SICF to potentially influence single-pulse MEP amplitudes (24).

Data Analyses

EMG.

EMG data were processed in Matlab (v.R2017b, The MathWorks Inc., MA) and R-studio (R-core team, 2021). All EMG traces were visually inspected and discarded if any background muscle contraction was detected. On average 3.96% trials were discarded per participant and there were no differences between conditions (linear mixed effect model $P = 0.76$) or muscles ($P = 0.64$). Peak-to-peak amplitude of the MEP was calculated from the remaining trials in the interval 15–40 ms after the TMS pulse. The average MEP amplitude was calculated for each individual and within each muscle for either each ISI (SICF-curves) or for each stimulation position and condition (motor maps). Any target with a mean MEP amplitude <0.05 mV was interpreted as a nonresponse site and the MEP value set to 0 to exclude the contribution of background noise to the results.

Coefficient of variation.

An intrinsic property of the corticospinal system is the inverse relationship between MEP amplitude and relative trial-to-trial variability between responses [i.e., coefficient of variation (CV)] (25). Previous studies have shown that the variability of corticospinal excitability can track the state of action preparation (26, 27). This prompted us to assess whether CV of the three conditions would follow the same trajectory. We reasoned that conditions with different CV-MEP amplitude relationships would be more likely to originate from distinct networks. Inspired by previous studies (26, 27), we modeled the relationship between CV and mean log-transformed MEP amplitude for each map target with a mean MEP amplitude >0.05 mV in the S1 condition in a linear mixed effect model: $CV \sim \log(MEP_{amplitude}) + (1 + \text{muscle} \mid \text{subject})$. We used the coefficients from this model to predict the CV for all three conditions and calculated the residuals between the predicted and observed CV. The resultant CV residuals were used in further analyses.

MEP latencies.

Previous studies have shown that the anterior-posterior position of the MEP hotspot is associated with changes in MEP latency (18). Thus, differences in MEP latency between conditions could suggest the influence of different corticospinal networks. MEP latencies were estimated by visual inspection of mean traces from the S1 and individual $SICF_1$ and $SICF_2$ peaks from the SICF curves.

TMS motor maps.

Facilitatory effects of SICF mapping. The corticomotor representation of SICF was assessed as the area and volume of the generated maps. The area of the motor maps was computed as the number of TMS targets eliciting an average MEP response of above 50 μV. In addition, map volume was calculated as the sum of the mean MEP amplitude from each target position within each motor map. Map volume was calculated both from raw MEP amplitudes and normalized to the largest mean MEP of each map (i.e., "peak-normalized" volumes).

Center of gravity. TMS target positions were extracted from the neuronavigation software as 3-D coordinates and converted into MNI space using SPM affine matrix conformation. As the hand-knob is not aligned to any one axes in 3-D Cartesian space and because the grid of TMS targets closely resembled a plane, we reduced the dimensionality of the maps, by performing a principal component analysis on centered target-coordinates of each individual map. The resulting first two principal components were used to construct two-dimensional (2-D) maps where the first principal component (PC1) primarily represented the medio-lateral but also the dorso-ventral axis (referred to as the medio-lateral axis) and the second principal component (PC2) primarily represented the anterior-posterior axis. From the 2-D maps, we calculated the amplitude-weighted mean position (i.e., the CoG) for both principal components, using the following formula:

$$\text{CoG} = \frac{\sum_{k=1}^{21} \text{Target}(k) \times \text{Mean MEP amplitude target}(k)}{\sum_{k=1}^{21} \text{Mean MEP amplitude target}(k)},$$

where target(k) refers to the PC1 or PC2 coordinate for each of the 21 TMS target positions and mean MEP amplitude target(k) refers to the mean peak-to-peak MEP amplitude at each target. The CoG was computed for each condition (S1, $SICF_1$, and $SICF_2$) and for each muscle (FDI or ADM) separately. Along with CoG coordinates we also calculated the Euclidian distance between FDI and ADM CoGs for all three conditions, and within the FDI and ADM muscle between S1 and $SICF_1$ and $SICF_2$.

Statistical Analysis

Statistical analyses were carried out in R (R core team, 2021). For all analyses, linear mixed effect models were fitted using the *lme4* and *lmertest* packages (28, 29), and multiple comparisons and adjusted P values were computed using the *multcomp* package (30). Post hoc pairwise comparisons were corrected for multiple comparisons using the "single-step" method (30) unless stated otherwise and statistical significance was assumed if $P < 0.05$. Homoskedasticity and normality was assured by visual inspection of residual- and quantile-quantile plots, respectively. Log-transformation was applied to the dependent variable if any obvious deviations from these assumptions were detected. For SICF curves, the following model was tested: $\log(MEP_{amplitude}) \sim \text{muscle} \times \text{ISI} + (1 + \text{muscle} \mid \text{subject})$. P values were obtained from analysis of variance tables for the fixed effects on the full model using Satterhwaite's degrees of freedom method. In addition, we tested the models: $CoG_{PC1} \sim \text{muscle} \times \text{condition} + (1 + \text{muscle} \mid \text{subject})$ and $CoG_{PC2} \sim \text{muscle} \times \text{condition} + (1 + \text{muscle} \mid \text{subject})$ to test for differences in CoG and $\log(Map_{volume}) \sim \text{muscle} \times \text{condition} + (1 + \text{muscle} \mid \text{subject})$, $Map_{volume\ normalized} \sim \text{muscle} \times \text{condition} + (1 + \text{muscle} \mid \text{subject})$ and $Map_{area} \sim \text{muscle} \times \text{condition} + (1 + \text{muscle} \mid \text{subject})$ to test for differences in map area and volumes. Differences in Euclidean distance between- or within muscle were assessed with: $Euclidean_{within} \sim \text{condition} + (1 \mid \text{subject})$ and $Euclidean_{between} \sim \text{condition} + (1 \mid \text{subject})$. Differences in the relationship between CV and MEP amplitude was assessed with a linear mixed model: $CV_{residuals} \sim \text{condition} + (1 + \text{muscle} \mid \text{subject})$ and differences in MEP latency with: $MEP_{latency} \sim \log(MEP_{amplitude}) + \text{condition} + (1 + \text{muscle} \mid \text{subject})$.

Sensitivity analyses.

To ensure that our results were not biased by the reduction of TMS targets into a plane, we performed the same analysis in 3-D Cartesian space on all three directions (i.e., $CoG_{anterior\text{-}posterior}$, $CoG_{medial\text{-}lateral}$, and $CoG_{ventral\text{-}dorsal}$ as outcome variables) and also on a simple 3 × 7 grid of equally spaced targets which did not consider the actual placement of TMS targets in relation to each other (i.e., CoG_{line} and CoG_{column} as outcome variables).

Since MEP amplitudes often increase exponentially, this could potentially affect the interpretation of the normalized map volume analysis. Therefore, we also conducted the analysis using $\log(x + 1)$ transformed MEP amplitudes prior to normalization.

Data Availability

Pseudonymized data can only be shared with a formal Data Processing Agreement and a formal approval by the Danish Data Protection Agency in line with the requirements of the GDPR.

RESULTS

Tabularized output from the statistical models is presented in Supplemental Tables S1.1–1.17.

SICF Curves

Biphasic paired-pulse TMS produced distinct SICF peaks around the two expected ISI intervals in all participants. Analysis of log-transformed MEP amplitudes from the SICF curves for the entire cohort showed no interaction between muscle and ISI (F_{11} =0.36, $P = 0.97$). There was, however, a main effect of muscle, with overall larger log-transformed MEP amplitudes in the FDI muscle ($F_1 = 6.06$, $P = 0.027$). There was also an ISI-dependent facilitation in log-transformed MEP amplitude ($F_{11} = 61.4$, $P < 0.001$). In accordance with previous work using monophasic or biphasic stimuli (11, 31), the post hoc pairwise comparisons showed that paired-pulse TMS at ISIs ranging from 1.0 to 1.8 ms and from 2.4 to 3.0 ms increased mean log-transformed MEP amplitude compared with MEPs evoked by a single TMS pulse (all $P < 0.001$) (Fig. 2*A*). The mode of $SICF_1$ peak latency was 1.4 ms (10 subjects) and 2.8 ms for $SICF_2$ latency (eight subjects) (Fig. 2*B*). Median relative facilitation for the $SICF_1$ peak was 379% (range: 174%–827%) for ADM and 367% (range: 149%–1008%) for FDI. Median $SICF_2$-peak MEP amplitudes were 457% (range: 235%–983%) relative to S1 for ADM and 418% (range: 176%–700%) for FDI (Fig. 2*C*). There were no significant differences in relative peak facilitation between SICF peaks or muscles ($P > 0.05$). Summary statistics of MEP amplitudes from individual $SICF_1$ and $SICF_2$ peak latencies and the S1-pulse alone are shown in Supplemental Table S2.

SICF Mapping of Corticomotor Representations of Intrinsic Hand Muscles

SICF mapping caused an anterior-to-posterior shift of the CoG for both muscles compared with the CoG revealed by single-pulse mapping without changing the medio-lateral distance between the CoGs of the FDI and ADM muscles (Fig. 3*A* and Fig. 5). Consequently, there were no significant interactions between condition and muscle in any of the models ($P > 0.39$). The magnitude of the anterior-to-posterior shift of the CoGs was positively associated with the peak latency in the $SICF_1$ condition (Fig. 3*C*). The longer the $SICF_1$ peak latency, the larger was the anterior-to-posterior shift of the CoGs ($P = 0.008$). This was not the case for the $SICF_2$ condition.

Effects of condition on CoG location.

The linear mixed model of PC2 (i.e., anterior-posterior axis) CoGs showed a strong effect of condition ($F_2 = 18.29$, $P < 0.001$). Post hoc analysis showed that CoGs of both, the FDI and ADM muscles, were located more posterior during $SICF_2$ mapping compared with S1 (β estimate +/− standard error; 0.62 +/− 0.21, $P = 0.01$). Importantly, $SICF_1$ CoGs were even more posterior compared with both, the CoGs during single-pulse (1.28 +/− 0.21, $P < 0.001$) and $SICF_2$ mapping (0.66 +/− 0.21, $P = 0.005$). Along the PC1-axis, there was no effect of stimulation condition on CoG location ($F_2 = 0.77$, $P = 0.47$) (Fig. 3, *A* and *B*). There were no differences in Euclidian distance between muscles or among the three stimulation conditions ($F_2 = 1.12$, $P = 0.34$).

Effects of muscle on CoG location.

Along the PC1-axis, all three mapping conditions showed medial to lateral separation of CoGs for the ADM and FDI muscles ($F_1 = 30.65$, $P < 0.001$) with the FDI muscle positioned more laterally than the ADM in agreement with previous TMS and functional MRI mapping studies (15, 16, 32). The CoGs of the FDI and ADM muscles also showed a non-significant difference along the PC2 axis ($F_1 = 3.68$, $P = 0.08$) with the CoG of the FDI muscle being more posteriorly positioned than the CoG of the ADM muscle (Fig. 4). Taken together, the data show that the peak corticomotor representations of FDI and ADM, as indexed by the CoG, shifted in the anterior-to-posterior direction on the precentral gyrus during SICF mapping relative to single-pulse mapping, while maintaining their relative positions in the anterior-posterior and medio-lateral dimension (Fig. 5).

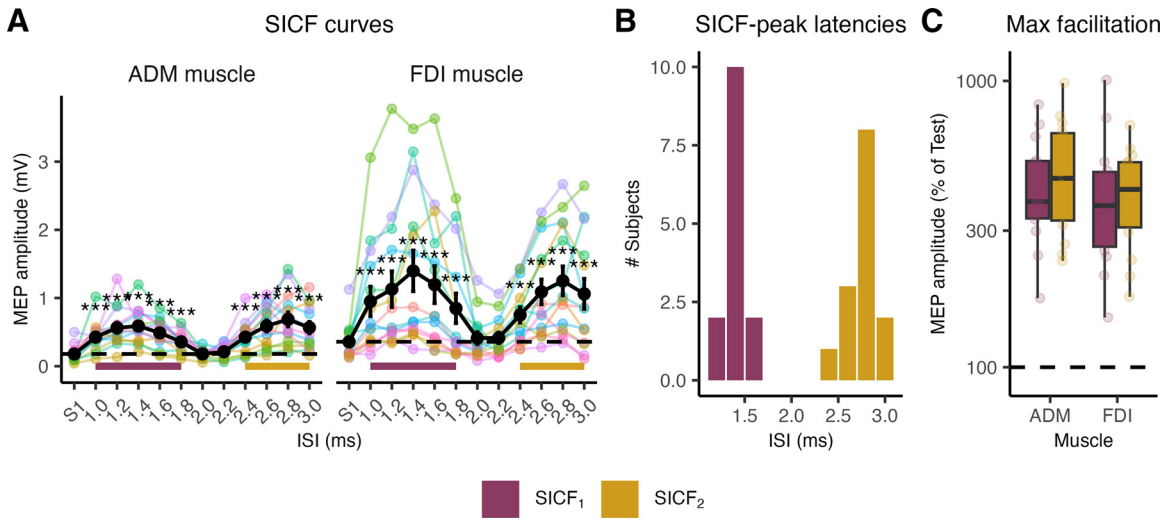

Figure 2. Short-latency intracortical facilitation (SICF) curves and individual SICF-peak latencies. *A*: individual (color) and mean (black) SICF curves for the abductor digiti minimi (ADM, *left*) and first dorsal interosseous (FDI, *right*) muscle. *B*: SICF-peak interstimulus intervals. *C*: individual maximum facilitation for each SICF-peak, relative to single-pulse (S1) stimulus. ***linear mixed effect model $P < 0.001$. ISI, interstimulus interval; MEP, motor-evoked potential.

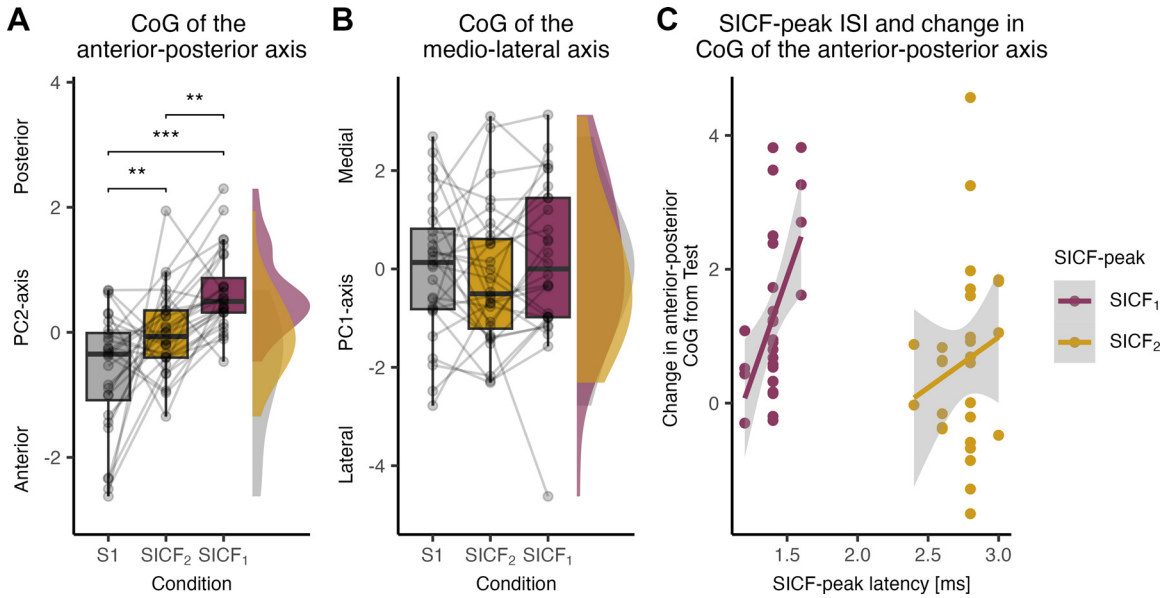

Figure 3. Effects of condition on the center of gravity (CoG). Point, box, and density plots of raw values of within-subject mean adjusted center of gravity of the anterior-posterior axis (*A*) and of the medio lateral axis (*B*). *C*: relationship between individual short-latency intracortical facilitation (SICF)-peak interstimulus interval (ISI) and changes in center of gravity of the anterior-posterior axis. Each point represents data from one muscle [abductor digiti minimi (ADM) or first dorsal interosseous (FDI)] for one participant. PC1, first principal component; PC2, second principal component. **linear mixed effects model $P < 0.01$, ***linear mixed effects model $P < 0.001$.

Sensitivity analyses.

The sensitivity analyses yielded similar results as our primary analysis, showing a separation of the two muscles in all three axes for the 3-D map and both axes on the simple grid map ($P < 0.05$). Interestingly, we found that the FDI muscle was more posterior on the grid map, whereas it was more anterior in 3-D Cartesian space reflecting that the central sulcus also runs in a posterior to anterior direction. These analyses also showed a separation of the three conditions across the three lines on the simple grid map ($P < 0.05$) (i.e., AP direction) and along the actual AP direction in 3-D Cartesian space ($P < 0.05$).

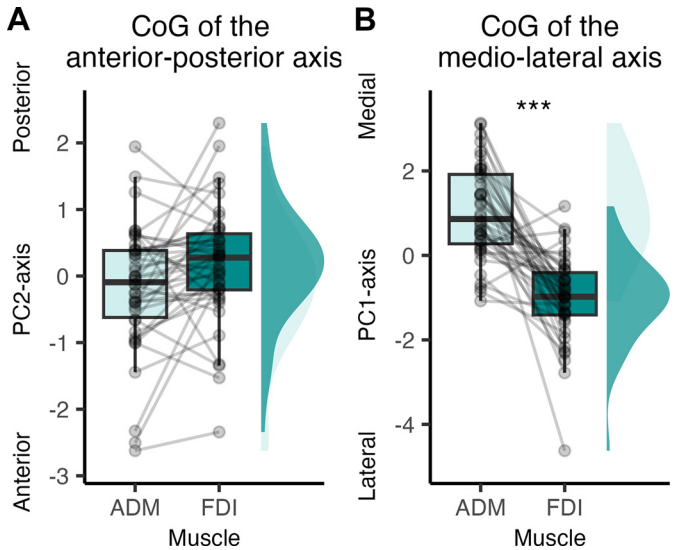

Figure 4. Effects of muscle on center of gravity (CoG). Point, box, and density plots of raw values of within-subject mean adjusted center of gravity for all three conditions of the anterior-posterior axis (*A*) and the medio lateral axis (*B*). Each point represents data from one condition [single-pulse (S1), short-latency intracortical facilitation ($SICF)_1$ or $SICF_2$] from one participant. ***linear mixed effects model $P < 0.001$. ADM, abducter digiti minimi; FDI, first dorsal interosseous; PC1, first principal component; PC2, second principal component.

Relationship between CoG Shift and SICF-Peak Latencies

We conducted mixed linear models with stimulation condition and muscle as fixed effects, subject as a random effect, and the difference in CoG along the anterior-posterior PC2-axis as the outcome variable, for each SICF condition separately. These models tested the hypothesis that the spatial shift in CoG position between SICF and single-pulse maps scaled linearly with individual SICF-peak latencies. For $SICF_1$ mapping, we found a positive linear relationship between $SICF_1$-peak latency and the relative shift in CoG during $SICF_1$ mapping (Fig. 3*C*). The larger the anterior-to-posterior shift in $SICF_1$ CoG relative to single-pulse stimulation, the longer was the individual $SICF_1$ latency [$F(1) = 9.45$, $P = 0.008$]. The $SICF_1$ model showed no effect of muscle and no interaction between muscle and stimulation condition ($P > 0.47$). For $SICF_2$ mapping, there was no linear relation between $SICF_2$-peak latency and the relative shift in CoG during $SICF_2$ mapping.

Effects of SICF Mapping on Map Excitability

As expected, area and log-transformed volume of both SICF maps were larger than the single-pulse map. Moreover, the volume of the peak-normalized SICF maps was larger than the peak-normalized single-pulse map suggesting an expansion of the motor representation independent of the amplitude facilitation.

SICF mapping map area increased from 7.6 ± 3.37 (mean ± standard deviation) active targets, to 10.93 ± 3.11 for the $SICF_2$ ($P < 0.001$) and 13.25 ± 2.98 for the $SICF_1$ ($P < 0.001$ compared

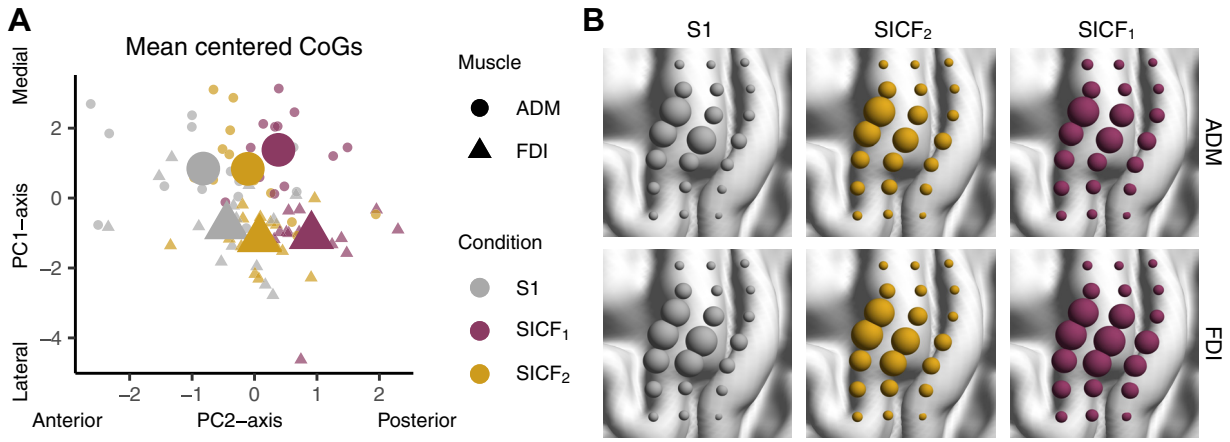

Figure 5. Center of gravity (CoG) and motor-evoked potential (MEP) amplitude distribution. *A*: individual (small) and mean (large), within-subject mean adjusted center of gravity in the first principal component (PC1) and second principal component (PC2) axes. *B*: bubble plots of mean peak-normalized MEP amplitudes for each condition and muscle. Each bubble represents the mean location of a map target in MNI space overlaid a three-dimensional (3-D) surface rendering of the ICBM152 brain in MNI space. Bubble size represent MEP amplitude relative to the maximum MEP amplitude for each condition and each muscle. Bubble plots were made using BrainNet Viewer (https://www.nitrc.org/projects/bnv/). Figures are for visualization purposes only. ADM, abductor digiti minimi; FDI, first dorsal interosseous; S1, single-pulse; SICF, short-latency intracortical facilitation.

with both S1 and $SICF_2$) (Fig. 6). For log-transformed map volume there was no interaction between muscle and condition ($F_2 = 1.15$, $P = 0.32$), but there was a significant main effect of muscle with FDI having a larger log-transformed map volume than ADM ($F_1 = 9.73$, $P = 0.008$). We also saw a significant effect of condition ($F_2 = 107.15$, $P < 0.001$), where log-transformed $SICF_2$ map volume was larger than log-transformed S1 volume ($1.19 +/- 0.11$, $P < 0.001$) and log-transformed $SICF_1$ map volume was larger than S1 ($1.48 +/- 0.11$, $P < 0.001$) and $SICF_2$ ($0.29 +/- 0.11$, $P = 0.021$). The results were similar for the peak-normalized maps, i.e., the relative map volume was larger for FDI compared with ADM ($F_1 = 9.8$, $P = 0.007$), and the relative map volume was larger for both $SICF_1$ and $SICF_2$ mapping compared with S1 ($P < 0.001$), but not between the two conditions ($P = 0.09$). Sensitivity analyses with $\log(x + 1)$ transformed MEP amplitudes prior to normalization also yielded results consistent with the original analysis with the exception of a statistically significant difference between $SICF_1$ and $SICF_2$ map volumes ($SICF_1 - SICF_2 = 0.64$, $P = 0.004$). Together, these results show that SICF stimulation results in a relative expansion of the corticomotor representation compared with single-pulse TMS, and this relative expansion was still present after accounting for differences in peak amplitude (i.e., peak corticospinal excitability).

Latency and CV Differences between Conditions

The linear relationship between CV and log-transformed MEP amplitudes was statistically significant ($P < 0.001$) and was captured by the following model: $CV = -0.131 \times \log(MEP_{amplitude}) + 0.776$. To assess whether the relationship between CV and MEP amplitude was similar between the three conditions, we modeled the residuals between the predicted and observed CV. We found a significant effect of condition [$F(2) = 6.15$, $P = 0.002$]. Post hoc tests showed that both $SICF_1$ and $SICF_2$ had lower CV residuals than the S1 condition ($SICF_1$: $-0.98 +/- 0.033$, $P = 0.009$; $SICF_2$: $-0.11 +/- 0.034$, $P = 0.003$), but there were no differences between $SICF_1$ and $SICF_2$ conditions ($P = 0.86$). We did not find any differences in MEP latency between the three conditions ($P = 0.7$) (Fig. 7).

DISCUSSION

Sulcus-aligned corticomotor mapping of intrinsic hand muscles revealed that SICF produces a posterior shift in corticomotor representation compared with single-pulse TMS, while preserving the well-known medial-to-lateral somatotopic gradient (16, 33). We also found a spatial discordance in CoGs between $SICF_1$- and $SICF_2$ maps, with $SICF_1$ CoGs located more posteriorly in the precentral crown. Finally, exploratory correlational analyses revealed a spatiotemporal relationship between the posterior shift of $SICF_1$ CoG and individual $SICF_1$ ISI. Our findings were supported by differences in the relationship between CV and log-transformed MEP amplitudes between S1 and SICF conditions.

Sulcus-Shaped Mapping Reveals Spatially Distinct Networks Mediating SICF

By aligning stimulation targets to the central sulcus and ensuring that the principal current direction is perpendicular to the gyral wall, even small spatial differences between intrinsic hand muscles are detectable (16). This type of sulcus-shaped mapping is highly sensitive to learning-dependent plasticity (34) and can be used to probe the intricate organization of the primary motor cortex (15) including interindividual differences in the anterior-posterior location of single-pulse TMS CoGs (18). We extend these previous findings by showing that sulcus-shaped mapping can reveal spatially distinct corticomotor maps from single- and paired-pulse TMS protocols.

Computational modeling show that TMS primarily activates cortical layers 2–5 in the gyral crown, with layer 5 pyramidal neurons having the lowest threshold followed by layer 2/3 pyramidal interneurons (2). Moreover, at perithreshold intensities, as applied in this study, direct waves are typically not observed epidurally (5). Thus, TMS pulses applied in this study therefore likely exerts its excitatory

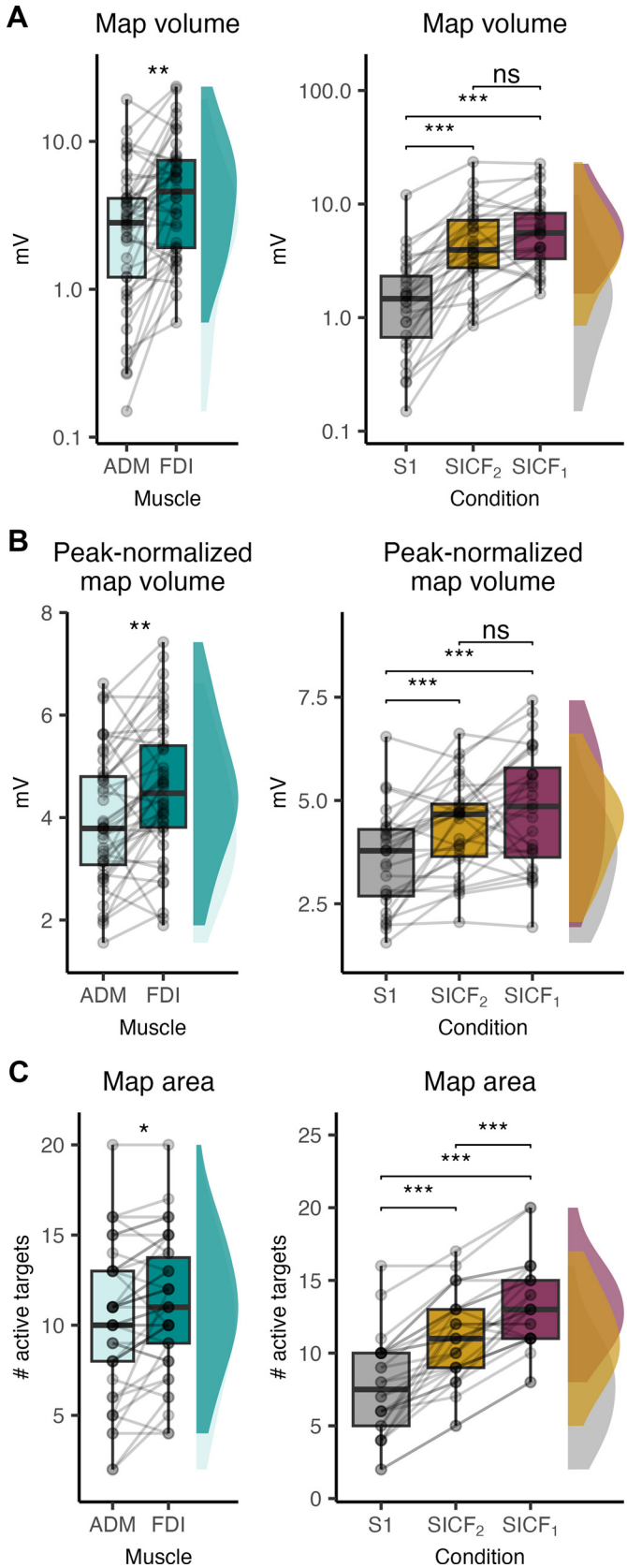

effect on PTNs indirectly through layer 2/3 and 5 pyramidal neurons located in the gyral crown or lip. Early work in animals has demonstrated that I-waves can be triggered from both parietal and premotor sites and the supplementary motor area (SMA) (35–37). Recent evidence also suggests a tight coupling between somatosensory high-frequency oscillations, SICF periodicity, and cortical somatosensory myelination in humans (38). Based on this coupling combined with the notion that TMS directed at the precentral gyrus evokes an (almost) equally strong electric field in the primary somatosensory area (1), one hypothesis could be that the posterior shift in SICF hotspot is brought about through coactivation of the primary somatosensory area.

Nevertheless, the only factor separating single-pulse and SICF conditions in the current study is the subthreshold pulse (S2) applied in SICF, which is thought to act on cortical elements excited by the suprathreshold S1 pulse (8). Thus, one interpretation of our results is that the subthreshold S2 SICF pulse causes suprathreshold excitation of neurons in the subliminal fringe of the S1, which are located posterior to neurons excited by low-intensity suprathreshold single-pulse TMS.

The relationship between SICF and I-waves is still not known. When two low-intensity pulses with 1–1.4 ms, but not 2 ms, ISI are applied, the number and size of descending waves recorded epidurally and the ensuing MEP increases (10). However, the use of two suprathreshold stimulations limits the interpretation as the S1 could be acting on S2 rather than the other way around. As such, although SICF and corticospinal I-waves likely originate at least in part from the same circuitry, the neural underpinnings are still not known. Recent methodological advancements enable the mapping of immediate TMS-evoked EEG activity and may pave the wave for future exploration of this matter (39). Additional support for our hypothesis that SICF is mediated by distinct networks, was found when analyzing differences in CV residuals based on the modeled relationship between CV and log-transformed MEP amplitude from the S1 condition (26). We found that CV residuals were lower for both SICF conditions. This means that the trial-to-trial MEP variability was lower for SICF conditions than what would have been expected from single-pulse TMS eliciting MEPs at a similar amplitude. This may be accounted for by SICF producing more synchronized descending activity than single-pulse TMS, supporting the notion that single-pulse MEPs and SICF is produced by nonidentical networks. On the other hand, we did not find any differences in MEP latency between single-pulse and the two SICF peaks measured from the SICF curves. A previous study has shown that more anterior hotspots were associated with longer MEP latency (18). Therefore, we would have expected the posterior shift in CoG in SICF conditions to have resulted in shorter MEP latencies, which we did not see. One reason for this could be

Figure 6. Short-latency intracortical facilitation (SICF) map facilitation. Point, box, and density plots of differences between muscles for all three conditions (*left*) and between conditions for both muscles (right) on raw values of map volume (*A*), within map peak-normalized map volume (*B*), and map area (*C*). Each point represents data from one muscle [abductor digiti minimi (ADM) or first dorsal interosseous (FDI)] or one condition [single-pulse (S1), $SICF_1$ or $SICF_2$] from one participant (left and right side respectively). *linear mixed effects model $P < 0.05$, **linear mixed effects model $P < 0.01$, ***linear mixed effects model $P < 0.001$.

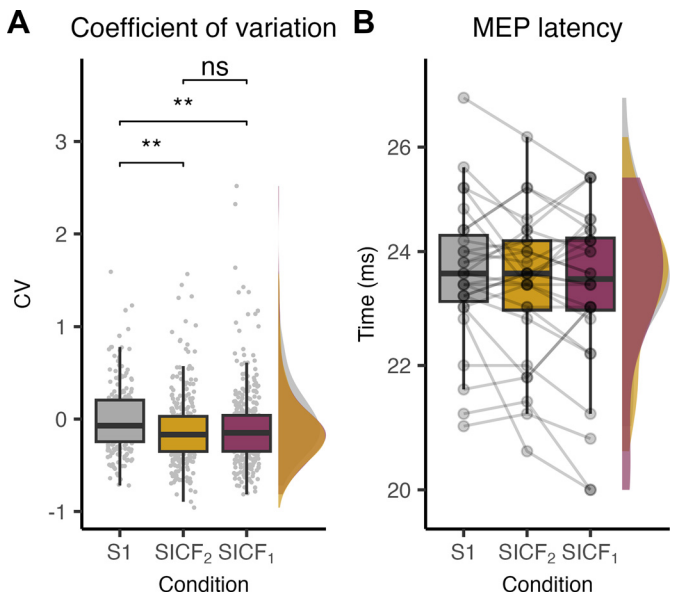

Figure 7. Coefficient of variation and motor-evoked potential (MEP) latency. Point, box, and density plots of differences in coefficient of variation (CV) residuals (*A*) and MEP latency (*B*) between the three conditions. In (*A*) each point reflects the difference between predicted and observed CV for each stimulation target for each participant and each condition. In (*B*) each point represents data from one muscle from one participant. **linear mixed effects model $P < 0.01$, ns, not significant. SICF, short-latency intracortical facilitation.

that in the SICF paradigm the S2 is believed to cause facilitation of S1 meaning that S1 dictates the MEP latency whereas S2 only influences later descending activity. However, future studies should investigate the relationship between MEP latency and paired-pulse TMS further.

$SICF_1$ and $SICF_2$ Peaks Are Generated by Spatially Distinct Networks

Electrophysiological experiments have shown that conditioning SICF with a subthreshold stimulation prior to the S1 stimuli (i.e., SICI conditioning) produces specific modulation of only the second SICF peak (40). This suggests that distinct interneuronal networks mediate the two first SICF peaks. Supporting this notion, only the $SICF_2$ peak is modulated during movement preparation (12, 41) and low-level contractions (13) and is facilitated after motor practice (14). We found a systematic spatial difference in $SICF_1$ and $SICF_2$ CoGs corroborating these previous findings and further suggesting that the two peaks are distinct phenomena generated by two spatially overlapping, but nonidentical networks.

Given the previously observed coupling between cortical myelination and SICF periodicity (38), we expected a linear relationship between the temporal distance of SICF peaks and the spatial shift in CoG. Interestingly, we found that the spatial shift of the $SICF_2$ peak was smaller than the earlier $SICF_1$ peak. This could reflect that $SICF_2$ is mediated either by *1*) slower conducting unmyelinated interneurons, *2*) additional interneuronal links, or *3*) that the $SICF_2$ peak is generated from multiple stimulated sites. Our method is not sensitive enough to dissociate these possibilities, but since we did not find a spatiotemporal relationship between individual $SICF_2$ CoG displacement and $SICF_2$ peak latency, this could indicate $SICF_2$ is influenced by multiple stimulated sites. On the contrary, our exploratory analysis did show a positive relationship between the posterior shift of $SICF_1$ CoG and individual $SICF_1$-peak ISI. This finding suggests that the longer the projection distance between the $SICF_1$ generating network and the hotspot for single-pulse TMS, the longer the conduction time. However, further research is needed to support this claim.

Short-Latency Paired-Pulse TMS Facilitates MEP Amplitude and Expands the Corticomotor Map

In line with a previous study from preoperative patients, SICF mapping produced both increased log-transformed map volume and expansion of the map area (42). However, the only study to investigate SICF in neurologically intact humans did not find any change in map area or spatial differences in map CoGs between single-pulse and SICF (43). Although the methodological approach was very similar to the current study, the authors used fixed ISIs of 1.4 and 2.8 ms and adjusted the S1 intensity for SICF to the paired-pulse threshold. This rendered both pulses below RMT meaning that it is unlikely that the S1 stimulus would be sufficiently strong to reveal any spatial differences between the conditions.

Interestingly, our data showed that map expansion was not contingent on the increase in MEP amplitude, but that the spatial extent of intracortical networks underlying SICF exceeds those activated from a single peri-threshold stimulation. Importantly, the map expansion cannot be attributed to an alteration of the induced e-field caused by applying paired-pulse TMS, as the temporal duration of a TMS-induced e-field is significantly shorter than the ISI of the paired pulses. This has important implications for the use of TMS. First, map expansion suggests that the spatial extent of the neural response to TMS in the stimulated cortex is influenced not only by the spatial properties of the induced electric field but also by physiological processes triggered by TMS. Second, map expansion indicates that single-pulse TMS mapping may not fully reveal the extent of the motor eloquent area, which could be particularly relevant for clinical applications such as preoperative TMS mapping (42, 44). More research is needed to dissociate whether map expansion is caused by recruitment of a spatially larger network, a better synchronization of descending corticospinal volleys, or both.

Methodological Considerations

In this study, we used biphasic AP-PA TMS pulses that is associated with a low corticomotor threshold (21), and enabled us to use lower stimulation intensities compared with monophasic pulses, minimizing the spatial spread of the induced electric field. Computational modeling of monophasic and biphasic TMS pulses suggest that the posterior lip of the precentral gyrus is more sensitive to the component of the stimulus producing a PA current direction (2). Moreover, monophasic AP- and PA-oriented pulses may target different I-wave generating networks (45) and potentially also different SICF peaks (46, 47). This could explain the spatial difference between single-pulse and SICF representations, as PA-sensitive neurons in the subliminal fringe could shift the SICF hotspot further posterior. On the other hand, epidural recordings show that I-waves from biphasic AP-PA stimulation occur at

the same latency as monophasic PA stimulation (48) and biphasic paired-pulse TMS elicits a characteristic SICF curve (31). These findings suggest that at least at near-threshold intensities, bi- and monophasic TMS target similar networks. Future studies should aim toward SICF mapping using monophasic pulses if possible.

An inherent limitation in the assessment of corticomotor excitability via compound potentials such as the MEP is the inability to segregate between direct monosynaptic inputs from corticomotoneuronal cells versus di-or polysynaptic inputs via brainstem or spinal interneurons. Consequently, we cannot reject the possibility that other descending pathways than the direct corticomotor projections influenced the observed facilitation and posterior shift in excitability profiles associated with the two SICF conditions. It should be noted that with peri-threshold stimulation intensities it is unlikely that brainstem pathways, such as the reticulospinal pathway, contribute to a meaningful extent to MEPs recorded from a quiescent hand muscle contralateral to the stimulated hemisphere (49–51).

Sulcus-shaped mapping is well established and has proven more sensitive to muscle somatotopy than simple grid-based mapping (16, 18, 34), but it does not allow for delineation of the effective cortical site or sites of TMS activation. When interpreting the CoG from TMS maps, it is crucial to recognize that the CoG method is inherently insensitive to multiple spatial peaks in corticomotor representations of a given muscle. Gordon et al. (52) used task-based functional MRI and phase mapping to delineate motor representations in the human brain, revealing a concentric organization of hand movements along the posteromedial-anterolateral axis. Our TMS mapping approach sampled a limited area and the sampling density of the stimulated grid, together with our CoG approach precludes the possibility of multiple peaks or hotspots of muscle representations. However, since our mapping procedure was identical between all conditions we are still able to make conclusions about the relative sites of TMS activation. Novel TMS mapping techniques that combines MEP measures with numerical modeling of induced electric fields have been developed (53–55), which could help elucidate this in future studies.

We used the FDI hotspot to determine SICF-peak latencies. This hotspot may not fully align with the CoG derived from the sulcus-shaped mapping and could potentially influence the SICF-peak latencies. However, similar spatial patterns were observed for SICF of the FDI and ADM despite their different spatial cortical representations. This between-muscle replication suggests that minor spatial discrepancies between the FDI hotspot and the CoGs of SICF were not critical. The possibility of different SICF-peak latencies at different pericentral sites is a relevant area of future research for which a multilocus TMS device would be ideal (56). The three TMS maps were generated separately. Since the amplitude but potentially also the type of the previous stimulation (24) may influence the corticomotor response to TMS, the magnitude of SICF may differ from the facilitation observed when SICF and S1 conditions are intermixed. Future studies should aim at investigating the effects of blocked versus interleaved SICF paradigms.

An additional limitation of the study is that the maps were only created at rest. SICF is still present during low level contractions, but we do not know how motor maps would be affected.

Conclusions

Shape-based TMS mapping of precentral motor cortex revealed that single-pulse TMS and SICF engages overlapping, but distinct corticomotor representations of intrinsic hand muscles. This spatial discordance supports the notion that the cortical elements that are most responsive to a single TMS pulse differ from those activated when probing SICF with paired-pulse TMS, revealing yet another facet of the finely arranged organization of the human motor cortex.

DATA AVAILABILITY

Source data for this study are not publicly available due to privacy or ethical restrictions. The pseudonymized data can only be shared with a formal Data Processing Agreement and a formal approval by the Danish Data Protection Agency in line with the requirements of the GDPR.

SUPPLEMENTAL MATERIAL

Supplemental Tables S1.1–S1.17: https://doi.org/10.6084/m9.figshare.28284521.v1.

Supplemental Table S2: https://doi.org/10.6084/m9.figshare.28284533.v1.

GRANTS

This work was supported by the Novo Nordisk Foundation Interdisciplinary Synergy Program “Biophysically adjusted state-informed cortex stimulation (BASICS) under Grant No. NNF14OC0011413. Lasse Christiansen holds a personal grant from the Lundbeck Foundation under Grant No. R322-2019-2406. Hartwig R. Siebner was supported by a collaborative research grant from Lundbeck Foundation HRS under Grant No. R336-2020-1035.

DISCLOSURES

Hartwig R. Siebner has received honoraria as speaker and consultant from Lundbeck AS, Denmark, and as editor (Neuroimage Clinical) from Elsevier Publishers, Amsterdam, The Netherlands. He has received royalties as book editor from Springer Publishers, Stuttgart, Germany, Oxford University Press, Oxford, UK, and from Gyldendal Publishers, Copenhagen, Denmark. None of the other authors has any conflicts of interest, financial or otherwise, to disclose.

AUTHOR CONTRIBUTIONS

M.A.J.M., C.C., M.G.J., and H.R.S. conceived and designed research; M.A.J.M., C.C., and M.G.J. performed experiments; M.A.J.M. analyzed data; M.A.J.M., L.C., and H.R.S. interpreted results of experiments; M.A.J.M. prepared figures; M.A.J.M. and L.C. drafted manuscript; M.A.J.M., L.C., C.C., M.G.J., and H.R.S. edited and revised manuscript; M.A.J.M., L.C., C.C., M.G.J., and H.R.S. approved final version of manuscript.

REFERENCES

1. **Thielscher A**, **Opitz A**, **Windhoff M.** Impact of the gyral geometry on the electric field induced by transcranial magnetic stimulation. *Neuroimage* 54: 234–243, 2011. doi:10.1016/j.neuroimage.2010.07.061.
2. **Aberra AS**, **Wang B**, **Grill WM**, **Peterchev AV.** Simulation of transcranial magnetic stimulation in head model with morphologically-realistic cortical neurons. *Brain Stimul* 13: 175–189, 2020. doi:10.1016/j.brs.2019.10.002.

3. **Siebner HR**, **Funke K**, **Aberra AS**, **Antal A**, **Bestmann S**, **Chen R**, **Classen J**, **Davare M**, **Di Lazzaro V**, **Fox PT**, **Hallett M**, **Karabanov AN**, **Kesselheim J**, **Beck MM**, **Koch G**, **Liebetanz D**, **Meunier S**, **Miniussi C**, **Paulus W**, **Peterchev AV**, **Popa T**, **Ridding MC**, **Thielscher A**, **Ziemann U**, **Rothwell JC**, **Ugawa Y.** Transcranial magnetic stimulation of the brain: what is stimulated?—a consensus and critical position paper. *Clin Neurophysiol* 140: 59–97, 2022. doi:10.1016/j.clinph.2022.04.022.
4. **Rathelot JA**, **Strick PL.** Subdivisions of primary motor cortex based on cortico-motoneuronal cells. *Proc Natl Acad Sci USA* 106: 918–923, 2009. doi:10.1073/pnas.0808362106.
5. **Di Lazzaro V**, **Oliviero A**, **Profice P**, **Saturno E**, **Pilato F**, **Insola A**, **Mazzone P**, **Tonali P**, **Rothwell JC.** Comparison of descending volleys evoked by transcranial magnetic and electric stimulation in conscious humans. *Electroencephalogr Clin Neurophysiol* 109: 397–401, 1998. doi:10.1016/s0924-980x(98)00038-1.
6. **Kujirai T**, **Caramia MD**, **Rothwell JC**, **Day BL**, **Thompson PD**, **Ferbert A**, **Wroe S**, **Asselman P**, **Marsden CD.** Corticocortical inhibition in human motor cortex. *J Physiol* 471: 501–519, 1993. doi:10.1113/jphysiol.1993.sp019912.
7. **Ferbert A**, **Priori A**, **Rothwell JC**, **Day BL**, **Colebatch JG**, **Marsden CD.** Interhemispheric inhibition of the human motor cortex. *J Physiol* 453: 525–546, 1992. doi:10.1113/jphysiol.1992.sp019243.
8. **Ziemann U**, **Tergau F**, **Wassermann EM**, **Wischer S**, **Hildebrandt J**, **Paulus W.** Demonstration of facilitatory I wave interaction in the human motor cortex by paired transcranial magnetic stimulation. *J Physiol* 511: 181–190, 1998. doi:10.1111/j.1469-7793.1998.181bi.x.
9. **Tokimura H**, **Ridding MC**, **Tokimura Y**, **Amassian VE**, **Rothwell JC.** Short latency facilitation between pairs of threshold magnetic stimuli applied to human motor cortex. *Electroencephalogr Clin Neurophysiol* 101: 263–272, 1996. doi:10.1016/0924-980x(96)95664-7.
10. **Di Lazzaro V**, **Rothwell JC**, **Oliviero A**, **Profice P**, **Insola A**, **Mazzone P**, **Tonali P.** Intracortical origin of the short latency facilitation produced by pairs of threshold magnetic stimuli applied to human motor cortex. *Exp Brain Res* 129: 494–499, 1999. doi:10.1007/s002210050919.
11. **Kesselheim J**, **Takemi M**, **Christiansen L**, **Karabanov AN**, **Siebner HR.** Multipulse transcranial magnetic stimulation of human motor cortex produces short-latency corticomotor facilitation via two distinct mechanisms. *J Neurophysiol* 129: 410–420, 2023. doi:10.1152/jn.00263.2022.
12. **Cattaneo L**, **Voss M**, **Brochier T**, **Prabhu G**, **Wolpert DM**, **Lemon RN.** A cortico-cortical mechanism mediating object-driven grasp in humans. *Proc Natl Acad Sci USA* 102: 898–903, 2005. doi:10.1073/pnas.0409182102.
13. **Ortu E**, **Deriu F**, **Suppa A**, **Tolu E**, **Rothwell JC.** Effects of volitional contraction on intracortical inhibition and facilitation in the human motor cortex. *J Physiol* 586: 5147–5159, 2008. doi:10.1113/jphysiol.2008.158956.
14. **Ho K**, **Cirillo J**, **Ren A**, **Byblow WD.** Intracortical facilitation and inhibition in human primary motor cortex during motor skill acquisition. *Exp Brain Res* 240: 3289–3304, 2022. doi:10.1007/s00221-022-06496-3.
15. **Dubbioso R**, **Raffin E**, **Karabanov A**, **Thielscher A**, **Siebner HR.** Centre-surround organization of fast sensorimotor integration in human motor hand area. *Neuroimage* 158: 37–47, 2017. doi:10.1016/j.neuroimage.2017.06.063.
16. **Raffin E**, **Pellegrino G**, **Di Lazzaro V**, **Thielscher A**, **Siebner HR.** Bringing transcranial mapping into shape: sulcus-aligned mapping captures motor somatotopy in human primary motor hand area. *Neuroimage* 120: 164–175, 2015. doi:10.1016/j.neuroimage.2015.07.024.
17. **Bashir S**, **Perez JM**, **Horvath JC**, **Pascual-Leone A.** Differentiation of motor cortical representation of hand muscles by navigated mapping of optimal TMS current directions in healthy subjects. *J Clin Neurophysiol* 30: 390–395, 2013. doi:10.1097/WNP.0b013e31829dda6b.
18. **Dubbioso R**, **Madsen KH**, **Thielscher A**, **Siebner HR.** The myelin content of the human precentral hand knob reflects interindividual differences in manual motor control at the physiological and behavioral level. *J Neurosci* 41: 3163–3179, 2021. doi:10.1523/JNEUROSCI.0390-20.2021.
19. **Oldfield RC.** The assessment and analysis of handedness: the Edinburgh inventory. *Neuropsychologia* 9: 97–113, 1971. doi:10.1016/0028-3932(71)90067-4.
20. **Rossi S**, **Hallett M**, **Rossini PM**, **Pascual-Leone A**; **Safety of TMS Consensus Group.** Safety, ethical considerations, and application guidelines for the use of transcranial magnetic stimulation in clinical practice and research. *Clin Neurophysiol* 120: 2008–2039, 2009. doi:10.1016/j.clinph.2009.08.016.
21. **Lang N**, **Harms J**, **Weyh T**, **Lemon RN**, **Paulus W**, **Rothwell JC**, **Siebner HR.** Stimulus intensity and coil characteristics influence the efficacy of rTMS to suppress cortical excitability. *Clin Neurophysiol* 117: 2292–2301, 2006. doi:10.1016/j.clinph.2006.05.030.
22. **Rossini PM**, **Burke D**, **Chen R**, **Cohen LG**, **Daskalakis Z**, **Di Iorio R**, **Di Lazzaro V**, **Ferreri F**, **Fitzgerald PB**, **George MS**, **Hallett M**, **Lefaucheur JP**, **Langguth B**, **Matsumoto H**, **Miniussi C**, **Nitsche MA**, **Pascual-Leone A**, **Paulus W**, **Rossi S**, **Rothwell JC**, **Siebner HR**, **Ugawa Y**, **Walsh V**, **Ziemann U.** Non-invasive electrical and magnetic stimulation of the brain, spinal cord, roots and peripheral nerves: basic principles and procedures for routine clinical and research application. An updated report from an I.F.C.N. Committee. *Clin Neurophysiol* 126: 1071–1107, 2015. doi:10.1016/j.clinph.2015.02.001.
23. **Yousry TA**, **Schmid UD**, **Alkadhi H**, **Schmidt D**, **Peraud A**, **Buettner A**, **Winkler P.** Localization of the motor hand area to a knob on the precentral gyrus. A new landmark. *Brain* 120: 141–157, 1997. doi:10.1093/brain/120.1.141.
24. **Bonnesen MT**, **Fuglsang SA**, **Siebner HR**, **Christiansen L.** The recent history of afferent stimulation modulates corticospinal excitability. *Neuroimage* 258: 119365, 2022. doi:10.1016/j.neuroimage.2022.119365.
25. **Darling WG**, **Wolf SL**, **Butler AJ.** Variability of motor potentials evoked by transcranial magnetic stimulation depends on muscle activation. *Exp Brain Res* 174: 376–385, 2006. doi:10.1007/s00221-006-0468-9.
26. **Klein-Flügge MC**, **Nobbs D**, **Pitcher JB**, **Bestmann S.** Variability of human corticospinal excitability tracks the state of action preparation. *J Neurosci* 33: 5564–5572, 2013. doi:10.1523/JNEUROSCI.2448-12.2013.
27. **Rao N**, **Parikh PJ.** Fluctuations in human corticospinal activity prior to grasp. *Front Syst Neurosci* 13: 77, 2019. doi:10.3389/fnsys.2019.00077.
28. **Bates D**, **Mächler M**, **Bolker B**, **Walker S.** Fitting linear mixed-effects models using lme4. *J Stat Soft* 67: 1–48, 2015. doi:10.18637/jss.v067.i01.
29. **Kuznetsova A**, **Brockhoff PB**, **Christensen RHB.** lmerTest package: tests in linear mixed effects models. *J Stat Soft* 82: 26, 2017. doi:10.18637/jss.v082.i13.
30. **Hothorn T**, **Bretz F**, **Westfall P.** Simultaneous inference in general parametric models. *Biom J* 50: 346–363, 2008. doi:10.1002/bimj.200810425.
31. **Kallioniemi E**, **Savolainen P**, **Järnefelt G**, **Koskenkorva P**, **Karhu J**, **Julkunen P.** Transcranial magnetic stimulation modulation of corticospinal excitability by targeting cortical I-waves with biphasic paired-pulses. *Brain Stimul* 11: 322–326, 2018. doi:10.1016/j.brs.2017.10.014.
32. **Lotze M**, **Erb M**, **Flor H**, **Huelsmann E**, **Godde B**, **Grodd W.** fMRI evaluation of somatotopic representation in human primary motor cortex. *Neuroimage* 11: 473–481, 2000. doi:10.1006/nimg.2000.0556.
33. **Wilson SA**, **Thickbroom GW**, **Mastaglia FL.** Transcranial magnetic stimulation mapping of the motor cortex in normal subjects. The representation of two intrinsic hand muscles. *J Neurol Sci* 118: 134–144, 1993. doi:10.1016/0022-510x(93)90102-5.
34. **Raffin E**, **Siebner HR.** Use-dependent plasticity in human primary motor hand area: synergistic interplay between training and immobilization. *Cereb Cortex* 29: 356–371, 2019. doi:10.1093/cercor/bhy226.
35. **Patton HD**, **Amassian VE.** Single and multiple-unit analysis of cortical stage of pyramidal tract activation. *J Neurophysiol* 17: 345–363, 1954. doi:10.1152/jn.1954.17.4.345.
36. **Amassian VE**, **Stewart M.** Motor cortical and other cortical interneuronal networks that generate very high frequency waves. *Suppl Clin Neurophysiol* 56: 119–142, 2003. doi:10.1016/s1567-424x(09)70214-4.
37. **Maier MA**, **Armand J**, **Kirkwood PA**, **Yang HW**, **Davis JN**, **Lemon RN.** Differences in the corticospinal projection from primary motor cortex and supplementary motor area to macaque upper limb motoneurons: an anatomical and electrophysiological study. *Cereb Cortex* 12: 281–296, 2002. doi:10.1093/cercor/12.3.281.

38. **Tomasevic L**, **Siebner HR**, **Thielscher A**, **Manganelli F**, **Pontillo G**, **Dubbioso R.** Relationship between high-frequency activity in the cortical sensory and the motor hand areas, and their myelin content. *Brain Stimul* 15: 717–726, 2022. doi:10.1016/j.brs.2022.04.018.
39. **Beck MM**, **Christiansen L**, **Madsen MAJ**, **Jadidi AF**, **Vinding MC**, **Thielscher A**, **Bergmann TO**, **Siebner HR**, **Tomasevic L.** Transcranial magnetic stimulation of primary motor cortex elicits an immediate transcranial evoked potential. *Brain Stimul* 17: 802–812, 2024. doi:10.1016/j.brs.2024.06.008.
40. **Shirota Y**, **Hamada M**, **Terao Y**, **Matsumoto H**, **Ohminami S**, **Furubayashi T**, **Nakatani-Enomoto S**, **Ugawa Y**, **Hanajima R.** Influence of short-interval intracortical inhibition on short-interval intracortical facilitation in human primary motor cortex. *J Neurophysiol* 104: 1382–1391, 2010. doi:10.1152/jn.00164.2010.
41. **Cretu AL**, **Ruddy KL**, **Post A**, **Wenderoth N.** Muscle-specific modulation of indirect inputs to primary motor cortex during action observation. *Exp Brain Res* 238: 1735–1744, 2020. doi:10.1007/s00221-020-05801-2.
42. **Zhang H**, **Julkunen P**, **Schröder A**, **Kelm A**, **Ille S**, **Zimmer C**, **Pitkänen M**, **Meyer B**, **Krieg SM**, **Sollmann N.** Short-interval intracortical facilitation improves efficacy in nTMS motor mapping of lower extremity muscle representations in patients with supra-tentorial brain tumors. *Cancers (Basel)* 12: 3233, 2020. doi:10.3390/cancers12113233.
43. **Pitkänen M**, **Kallioniemi E**, **Järnefelt G**, **Karhu J**, **Julkunen P.** Efficient mapping of the motor cortex with navigated biphasic paired-pulse transcranial magnetic stimulation. *Brain Topogr* 31: 963–971, 2018. doi:10.1007/s10548-018-0660-9.
44. **Sollmann N**, **Zhang H**, **Kelm A**, **Schröder A**, **Meyer B**, **Pitkanen M**, **Julkunen P**, **Krieg SM.** Paired-pulse navigated TMS is more effective than single-pulse navigated TMS for mapping upper extremity muscles in brain tumor patients. *Clin Neurophysiol* 131: 2887–2898, 2020. doi:10.1016/j.clinph.2020.09.025.
45. **Sommer M**, **Ciocca M**, **Chieffo R**, **Hammond P**, **Neef A**, **Paulus W**, **Rothwell JC**, **Hannah R.** TMS of primary motor cortex with a biphasic pulse activates two independent sets of excitable neurones. *Brain Stimul* 11: 558–565, 2018. doi:10.1016/j.brs.2018.01.001.
46. **Delvendahl I**, **Lindemann H**, **Jung NH**, **Pechmann A**, **Siebner HR**, **Mall V.** Influence of waveform and current direction on short-interval intracortical facilitation: a paired-pulse TMS study. *Brain Stimul* 7: 49–58, 2014. doi:10.1016/j.brs.2013.08.002.
47. **Opie GM**, **Semmler JG.** Preferential activation of unique motor cortical networks with transcranial magnetic stimulation: a review of the physiological, functional, and clinical evidence. *Neuromodulation* 24: 813–828, 2021. doi:10.1111/ner.13314.
48. **Di Lazzaro V**, **Oliviero A**, **Mazzone P**, **Insola A**, **Pilato F**, **Saturno E**, **Accurso A**, **Tonali P**, **Rothwell JC.** Comparison of descending volleys evoked by monophasic and biphasic magnetic stimulation of the motor cortex in conscious humans. *Exp Brain Res* 141: 121–127, 2001. doi:10.1007/s002210100863.
49. **Ziemann U**, **Ishii K**, **Borgheresi A**, **Yaseen Z**, **Battaglia F**, **Hallett M**, **Cincotta M**, **Wassermann EM.** Dissociation of the pathwaysmediating ipsilateral and contralateral motor-evoked potentials in human hand and arm muscles. *J Physiol* 518: 895–906, 1999. doi:10.1111/j.1469-7793.1999.0895p.x.
50. **Olivier E**, **Baker SN**, **Nakajima K**, **Brochier T**, **Lemon RN.** Investigation into non-monosynaptic corticospinal excitation of macaque upper limb single motor units. *J Neurophysiol* 86: 1573–1586, 2001. doi:10.1152/jn.2001.86.4.1573.
51. **Fisher KM**, **Zaaimi B**, **Baker SN.** Reticular formation responses to magnetic brain stimulation of primary motor cortex. *J Physiol* 590: 4045–4060, 2012. doi:10.1113/jphysiol.2011.226209.
52. **Gordon EM**, **Chauvin RJ**, **Van AN**, **Rajesh A**, **Nielsen A**, **Newbold DJ**, **et al.** A somato-cognitive action network alternates with effector regions in motor cortex. *Nature* 617: 351–359, 2023. doi:10.1038/s41586-023-05964-2.
53. **Numssen O**, **Zier AL**, **Thielscher A**, **Hartwigsen G**, **Knösche TR**, **Weise K.** Efficient high-resolution TMS mapping of the human motor cortex by nonlinear regression. *Neuroimage* 245: 118654, 2021. doi:10.1016/j.neuroimage.2021.118654.
54. **Weise K**, **Numssen O**, **Kalloch B**, **Zier AL**, **Thielscher A**, **Haueisen J**, **Hartwigsen G**, **Knösche TR.** Precise motor mapping with transcranial magnetic stimulation. *Nat Protoc* 18: 293–318, 2023. doi:10.1038/s41596-022-00776-6.
55. **Weise K**, **Numssen O**, **Thielscher A**, **Hartwigsen G**, **Knösche TR.** A novel approach to localize cortical TMS effects. *Neuroimage* 209: 116486, 2020. doi:10.1016/j.neuroimage.2019.116486.
56. **Nieminen JO**, **Koponen LM**, **Mäkelä N**, **Souza VH**, **Stenroos M**, **Ilmoniemi RJ.** Short-interval intracortical inhibition in human primary motor cortex: a multi-locus transcranial magnetic stimulation study. *Neuroimage* 203: 116194, 2019. doi:10.1016/j.neuroimage.2019.116194.